Preliminary similarity spectra analysis of noise from a high-performance trainer aircraft

Kristi A. Epps, Cooper D. Merrill, Aaron B. Vaughn, et al.

Citation: Proc. Mtgs. Acoust. **42**, 040006 (2020); doi: 10.1121/2.0001623
View online: https://doi.org/10.1121/2.0001623
View Table of Contents: https://asa.scitation.org/toc/pma/42/1
Published by the Acoustical Society of America

Volume 42 http://acousticalsociety.org/

179th Meeting of the Acoustical Society of America

Acoustics Virtually Everywhere

7-11 December 2020

Noise: Paper 4aNSc1

Preliminary similarity spectra analysis of noise from a high-performance trainer aircraft

Kristi A. Epps, Cooper D. Merrill, Aaron B. Vaughn, Kevin M. Leete and Kent L. Gee
Department of Physics and Astronomy, Brigham Young University, Provo, UT, 84602; kristi.epps5@gmail.com; cdouglasmerrill@gmail.com; aaron.burton.vaughn@gmail.com; kevinmatthewleete@gmail.com; kentgee@byu.edu

Alan T. Wall
Air Force Research Laboratory, Wright-Patterson Air Force Base, OH; alan.wall.4@us.af.mil

Because the noise source mechanisms and radiation properties associated with high-thrust, tactical jet engines are not fully understood, analysis of full-scale measurements can shed significant insight on such characteristics. One method for examining spectral data is to compare them to empirical models for jet noise spectra. This paper compares measured near-field spectra from a T-7A-installed GE F404-103 engine with analytical similarity spectra for fine-scale mixing noise, large-scale mixing noise, and broadband shock-associated noise. This initial similarity spectra analysis enables the determination of spatial trends in overall level and peak frequency and the relative importance of each type of noise radiation as a function of location. This approach can be used to gain insights on spatial and frequency trends of noise source mechanisms for different engine conditions and for rapid comparisons to other aircraft and jets of other scales and conditions.

Published by the Acoustical Society of America

 https://doi.org/10.1121/2.0001623

1. INTRODUCTION: JET NOISE PHENOMENA AND ANALYTICAL SPECTRA

Jet noise is generated when the turbulent exhaust of a jet engine mixes with the ambient air, creating broadband acoustic waves that, to some degree, radiate in all directions. Identification of military aircraft jet noise sources and characteristics may eventually enable improvement on noise reduction technologies.[1,2,3,4]

For a supersonic jet exhaust from a full-scale, installed engine, three main types of turbulence-induced noise[5,6] are believed to dominate, although other sources are being investigated.[7] Turbulent mixing noise consists of large-scale noise (LSN) radiated from large-scale, coherent structures and fine-scale noise (FSN) radiated from fine-scale turbulence. Additionally, because the jet is usually imperfectly expanded (overexpanded at takeoff), interaction of the large-scale turbulent structures with shock cells generates broadband shock-associated noise (BSN). Screech, a feedback-amplified tonal noise generated at the shock cells, has been studied at the laboratory-scale[8,9] but does not factor significantly in actual high-performance jet engine exhausts. Figure 1 shows a diagram of the jet and the three types of turbulent structures and their primary radiation characteristics. FSN is relatively spatially incoherent, and thus radiates in all directions. It tends to dominate upstream and to the sideline. On the other hand, LSN dominates at aft angles. When present, BSN preferentially radiates upstream and tends to be visible in the spectrum at angles that are dominated by FSN. However, it is more narrowband than FSN and with a greater peak frequency that increases with increasing inlet angle.

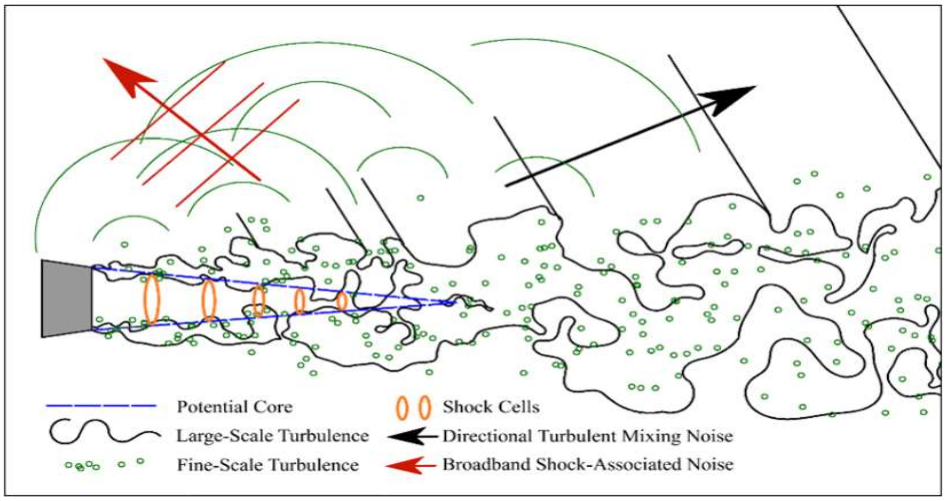

Figure 1. Diagram of jet noise and different source characteristics, created by Vaughn et al.[10]

Building on an assumption that both fine and large-scale turbulence contribute to the noise radiation from a jet, and that their spectral characteristics were likely different, Tam *et al.*[11] used several laboratory-scale datasets to develop fine-scale and large-scale similarity spectra models ($L_F(f)$ and $L_L(f)$, respectively). The $L_F(f)$ has a broad peak and round spectral shape, whereas the $L_L(f)$ has a narrower peak with power-law roll-up and roll-off that corresponds to greater temporal correlation.[12] Tam *et al.* compared these similarity spectra to the measured spectra ($L_p(f)$, represented as a power spectral density) to determine where the different turbulent structures appear. While these models were originally used to fit far-field laboratory-scale data, Neilsen *et al.*[13] found that they could also be used to reasonably fit near-field data from a high-performance, afterburner-capable tactical aircraft. Other full-scale similarity spectra analyses have been conducted[7,13,14,15] and have even been used to create level-based wavepacket models.[16]

Although not adopted nearly as extensively as Tam *et al.*'s $L_F(f)$ and $L_L(f)$, empirically derived, analytical models for BSN spectral shapes can also be incorporated into a similarity spectra analysis. This was done for noise from the F-35B by Neilsen *et al.*[14] using the model for BSN ($L_B(f)$) created by Kuo *et al.*[6] Whereas the $L_F(f)$ and the $L_L(f)$ have only two adjustable parameters – peak frequency and level – the $L_B(f)$ has an additional parameter that adjusts the spectral width. In order to eventually compare fits for different aircraft, the same fitting functions are used in the current analysis.

Tam *et al.*[15] also produced a model spectrum for BSN and similarly noted the need for three adjustable parameters for a BSN spectral model, but their use of the model was not in tandem with his other similarity spectra. By comparing the $L_F(f)$, $L_L(f)$, and $L_B(f)$ to the measured spectra, that it is possible to determine the sources of jet noise that contribute to the total measured spectrum at different observer locations. It is noted that fitting the $L_F(f)$, $L_L(f)$, and $L_B(f)$ to the $L_p(f)$ is done manually, and usually by committee. It is also an iterative process in that trends in fitting parameters and in resulting levels are expected to vary relatively smoothly. In this paper, preliminary fits to ground runup noise from the T-7A Red Hawk are described, to validate the approach used previously on the F-35.[14] We note that previous studies using Tam *et al.*'s similarity spectra have used nomenclature inconsistently (like "FSS" and "LSS"), resulting in confusion about whether a mixing noise phenomenon was being referred to, or the empirical spectral curves. This paper attempts to distinguish the mixing noise phenomena from the models used to identify their spectral characteristics, by defining a new nomenclature that clarifies which phenomenon or model is being referenced.

2. T-7A MEASUREMENTS

A. AIRCRAFT

The T-7A Red Hawk (see Figure 2) is a new high-performance trainer aircraft developed for the United States Air Force by Boeing. It has a single GE F404-103 engine that can produce about 11,000 kN (lbf) of thrust dry (17,000 kN (lbf) with afterburner). Variants of the F404 appear in single (KAI/LMTAS T-50) and twin-engine (F/A-18 C/D) tactical aircraft,[17] and its noise reduction has been studied by others.[1,2,3,4] Its derivative, the F414 engine, powers the F/A-18 E/F Super Hornet. Studying the noise radiation from this aircraft can help identify differences between single and twin-engine configurations and aid in further noise reduction efforts.

Figure 2. Image of the T-7A Red Hawk. Photo obtained from the DVIDS website: https://www.dvidshub.net/image/5754020/asecaf-announces-t-7a-red-hawk-during-air-space-and-cyber-conference

B. MEASUREMENT ENVIRONMENT

Measurements of the T-7A aircraft were taken on 18 August 2019 at Holloman Air Force Base in New Mexico. The measurements are described in detail by Leete *et al.*,[18] but salient details are repeated here. The aircraft was tied down to the pad with the nose pointing towards the jet blast deflector (see Figure 3a), to create an undeflected plume environment. The measurements were taken between 5AM and 7AM local time to avoid prevailing winds and limit their effect on the data. Six weather stations were set up to record ambient temperature, pressure, humidity, and wind speed and direction during the measurements at various locations in the area surrounding the runup pad.

C. RUNUPS

The engine was cycled through multiple engine conditions, which included various N2 values and maximum engine power. N2 refers to the rotational speed of an engine section associated with the high-pressure compressor. An ambient measurement was taken before beginning the engine startup. The Auxiliary Power Unit (APU) startup sequence, which supplies the air and electrical power necessary to turn on the aircraft, was then run and completed before the engine was started and run at idle. The engine was then run at 75%, 82%, 88%, military power (MIL), and afterburner with each engine condition running long enough for the data acquisition systems to record for thirty seconds before moving on to the next power level. After running at afterburner, the engine was brought down to idle for a few minutes to cool down before it was run through the same sequence again. Once the engine had finished running at afterburner for the second time, the engine was powered down before being started up a few minutes later. This whole process was repeated two more times, resulting in a total of six runups at each condition. In this preliminary analysis, limited results of only the 82% and afterburner engine conditions are shown.

D. MICROPHONE ARRAY

Although over 240 microphones were part of the measurements, only the results from some of those microphones along a 120-microphone near-field array are analyzed in this paper. The array was located on the left side of the aircraft, but subsequent diagrams of the microphone locations show them mirrored on the right side for plotting convenience. Microphone positions were defined in both Cartesian coordinates and inlet angle, relative to a microphone array reference position (MARP) located 3.96m (13ft) downstream of the nozzle. Given a nominal exit diameter of 0.51m (20 in), the MARP was located at 7.8 nozzle diameters. This same scaled MARP was used for prior aircraft analyses.[10,13,14,19]

The near-field ground array consisted of GRAS 1/4" 46BG and 46BD pressure and 46BE free-field microphones placed both upstream and downstream of the aircraft nozzle exit. They covered a range of inlet angles from 17.8° (upstream of the aircraft) to 165° (downstream of the aircraft). The microphones were oriented either pointed toward (46BE) or perpendicular (46BG and 46BD) to the MARP and taped to the ground, with the heads of the microphones placed on top of a strip of tape to prevent direct contact with the ground. Figure 3b shows part of this array facing downstream away from the jet blast deflector. Upstream of the nozzle, the array linearly increased in y for a short distance, and then ran parallel to the jet axis as shown in Figure 3c. Downstream of the nozzle, the array ran parallel to the approximated shear layer, starting at approximately 60° (about 0.8m aft of the nozzle) and extending away from the aircraft. The spacing between microphones was determined based on predicted peak frequencies and prior experience, which resulted in smaller spacing towards the sideline of the jet and larger spacing aft, where lower frequencies were predicted to dominate. The near-field ground array extends farther upstream and downstream with smaller average spacing than was used in previous measurements of other high-performance aircraft,[13,14] which allow for finer spatial resolution and frequency bandwidth in analyses. Pressure waveforms were synchronously recorded using a 24-bit National Instruments PXIe system, with a sampling rate of 204.8 kHz for all 120 channels.

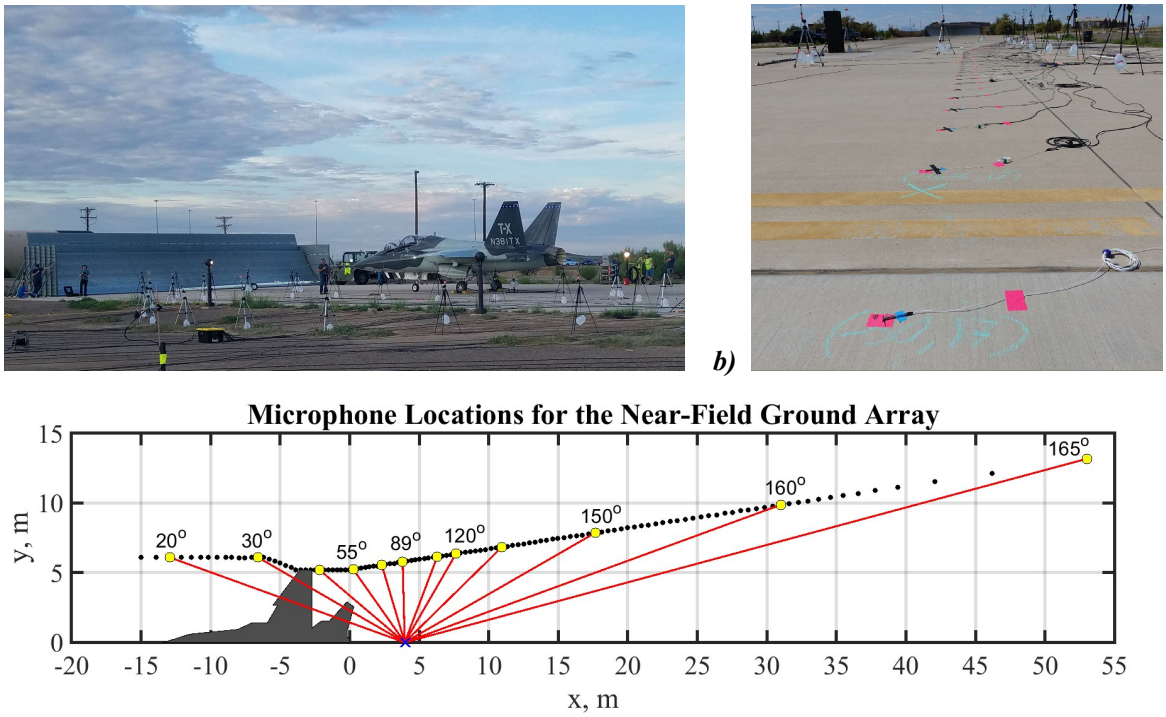

Figure 3. Images and diagram of the T-7A and near-field ground array: a) T-7A facing the jet blast deflector, b) near-field ground array microphone setup, pointing downstream, c) locations of the near-field ground array microphones relative to the aircraft, red lines and yellow markers indicate the microphones analyzed in later figures, MARP is indicated by the blue x.

3. RESULTS AND ANALYSIS

As this paper is an initial application of the $L_F(f)$,[11] the $L_L(f)$,[11] and the $L_B(f)$[6] to the T-7A measured spectra, spectral fits are only shown for two conditions: 82% N2 (50% of military power thrust) and afterburner. Spectral fits are shown at various inlet angles to portray the overall trends of the turbulence structures. These conditions and angles are sufficient to examine key phenomena identified in this dataset.

A. 82% N2

At angles upstream and to the side of the aircraft, the measured spectra at this intermediate engine condition exhibit broad, low-level peak behavior consistent with the characteristics of FSN. Tam *et al.*'s $L_F(f)$[11] is fitted to these spectra to confirm their fine-scale behavior. At locations very far upstream, the $L_F(f)$ is shown to match the middle frequencies of the $L_p(f)$ while greatly underestimating the levels of the low and high frequencies, as shown in Figure 4a. Engine tones are present at this location. As the inlet angle increases, the discrepancies at the low frequencies decrease until the $L_F(f)$ fits the measured spectra at both the low and middle frequencies. In Figures 4b and 4c, however, the high-frequency slopes of the $L_p(f)$ decrease such that there is a larger gap between the $L_p(f)$ and the $L_F(f)$. The disagreements seen at low and high frequencies at these upstream locations are likely caused by other engine-related noise sources besides FSN being present. With increasing inlet angle, the peak frequency of the $L_F(f)$ is found to decrease while the peak level tends to increase until approximately 92°, the angle at which the $L_L(f)$ is included, at which point the peak level of the $L_F(f)$ begins to decrease. These $L_F(f)$ trends match those found by Vaughn *et al.*[19] in their study on an unheated, Mach 1.8 laboratory-scale jet at both near- and mid-field locations. At 89° (Figure 4c), it could be argued that the $L_L(f)$ should be included to account for the taller peak that begins to appear at this location; however, in this analysis it is determined that the $L_F(f)$ is sufficient to fit most of the measured spectra.

Beginning at 92°, the measured spectra exhibit behaviors consistent with the characteristics of both FSN and LSN. At lower and higher frequencies, the slopes are shallow and broad, which match the FSN characteristics, whereas the peaks of the measured spectra are sharper than can be accounted for with the $L_F(f)$. The $L_L(f)$, which exhibits this peak behavior, is therefore essential to capturing the characteristics of FSN and LSN. Figure 4d,

which shows the $L_p(f)$, $L_F(f)$, and $L_L(f)$ at 111°, is an example of using both the $L_F(f)$ and $L_L(f)$ to capture the two different behaviors. The very low and high frequencies have shallower slopes than what Tam *et al.*'s models[11] predict, but the overall fit matches the $L_p(f)$ extremely well.

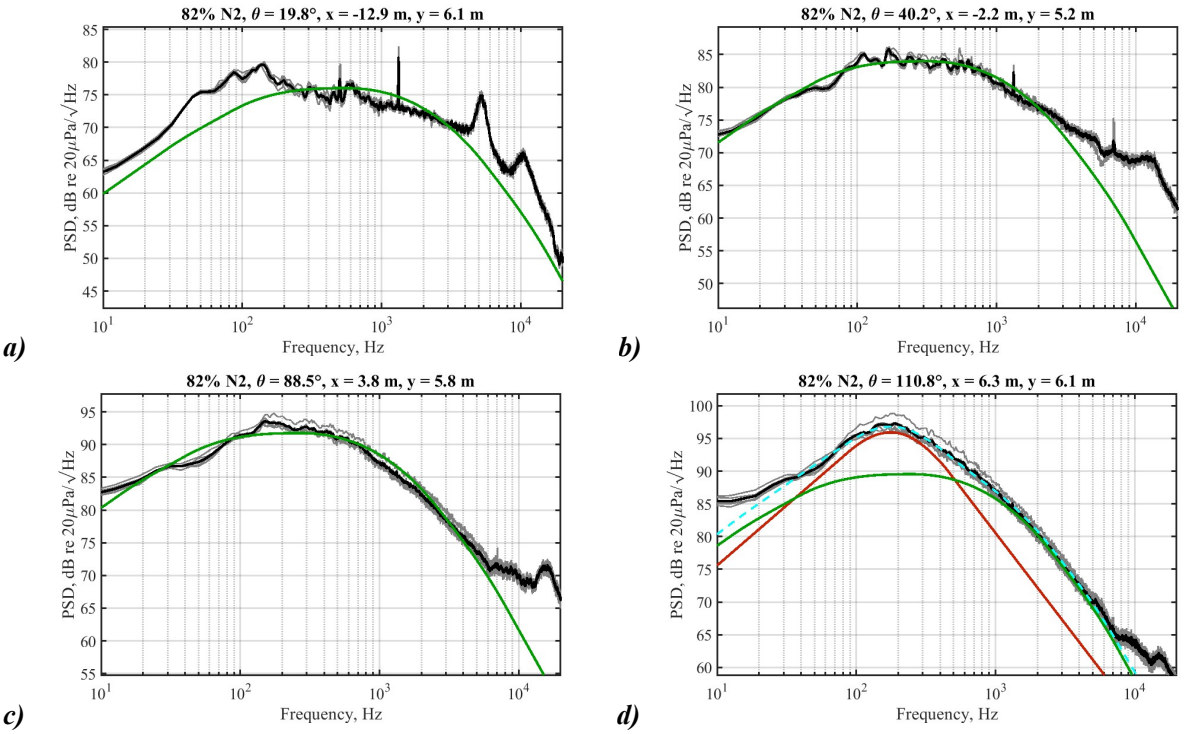

Figure 4. Measured and similarity spectra for 82% N2 consisting of gray lines ($L_p(f)$ of individual measurements), black lines ($L_p(f)$ of average of the 6 measurements), green lines ($L_F(f)$), red lines ($L_L(f)$), and cyan dashed lines (sum of $L_F(f)$ and $L_L(f)$) at angles of a) 20°, b) 40°, c) 89°, d) 111°.

As the inlet angle continues to increase, the characteristics of LSN become a more dominant part of the measured spectra until only the $L_L(f)$ is necessary to capture those characteristics. This transition occurs aft of 124°. Figure 5a shows that there is very good agreement between the $L_p(f)$ and the $L_L(f)$ immediately downstream of 124°. The lowest frequencies of the measured spectra have a shallower slope than the $L_L(f)$ predicts, but this is most likely due to saturation and, since the $L_L(f)$ very closely matches the levels at the other frequencies, does not affect the overall fit. Farther downstream, the $L_L(f)$ continues to agree with the slopes of the measured spectra, as is evident in Figure 5b. However, the peak of the $L_p(f)$ shifts to higher levels and frequencies than are predicted by the $L_L(f)$, and this trend continues from 138° to approximately 160°. This phenomenon has been absent in other analyses of noise from high-performance aircraft at the intermediate engine condition, and no known cause of their presence in this dataset has been identified or established. In examining the overall trends of the peak frequency and level of the $L_L(f)$ with increasing inlet angle, the peak frequency decreases while the peak level increases until approximately 137°, at which point the peak level begins to decrease. These trends were also observed by Vaughn *et al.*,[19] and they continue to the end of the array.

Near the end of the array, hydrodynamic effects due to the turbulent flow (rather than the radiated noise) are likely evident in the variability of the levels between each run and in the shapes of the measured spectra. In Figure 5c, the difference in level between each run is visible, but the shapes are still recognizable as those resulting from LSN, and thus the $L_L(f)$ is applied. As the measured spectra near the very end of the array are examined, their spectral shapes become much less defined. While it is noticeable that most of the runs exhibit behavior somewhat typical of LSN, the peak becomes too broad for the $L_L(f)$ to completely capture, as is shown in Figure 5d. With the addition of the two $L_p(f)$ whose shapes show very little resemblance to those of the other runs, it is nearly impossible to conclusively identify any LSN characteristics. Figure 5d shows the result of this analysis in applying the $L_L(f)$ to the $L_p(f)$ at the end of the array, but because it is difficult to find a strong resemblance to the $L_L(f)$ shape using the average $L_p(f)$, it is not firmly proposed that this is the most accurate

application of this analysis at this location. Whether the cause of such a lack of a distinct spectral shape is solely due to hydrodynamic effects or if there are other factors involved is not currently known.

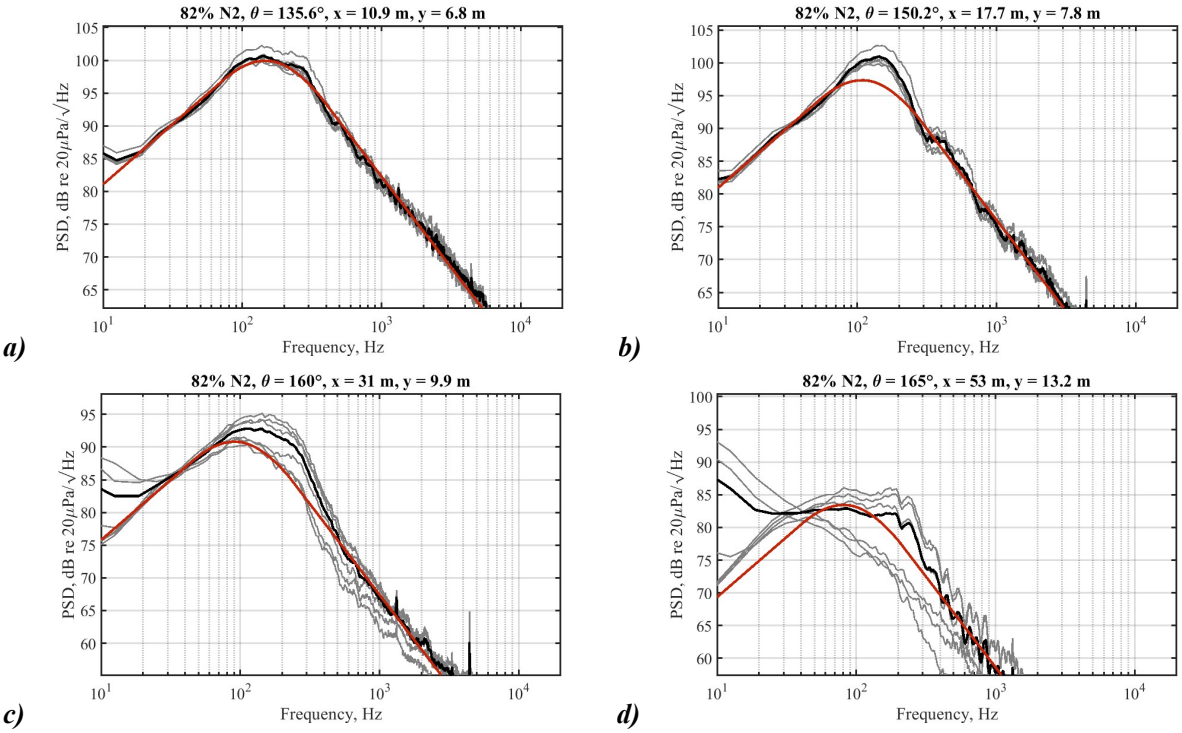

Figure 5. Measured and similarity spectra for 82% N2 consisting of gray lines ($L_p(f)$ of individual measurements), black lines ($L_p(f)$ of average of the 6 measurements), and red lines ($L_L(f)$) at angles of a) 136°, b) 150°, c) 160°, d) 165°.

B. AFTERBURNER

At higher engine conditions such as afterburner, spectral behavior typical of BSN characteristics is expected to appear at upstream and sideline angles and is, in fact, observed in this dataset. Figure 6a shows the narrow and sharp peak representative of BSN behavior as well as the broad peak and shallower slopes consistent with FSN, both of which can be represented with the $L_B(f)$ and the $L_F(f)$. These models, while matching the general trends and shape of the BSN and FSN characteristics, do not account for the various bumps and nulls seen across the whole spectrum. For the low frequencies especially, the $L_p(f)$ shows a shallower slope than the $L_F(f)$ predicts. As inlet angle increases, it is found that the peak level of the $L_F(f)$ steadily increases, whereas the peak frequency increases until approximately 52°, at which point it begins to decrease. The $L_F(f)$ must still be applied when BSN is present to match the broad peak not accounted for by the $L_B(f)$, but the slopes of the $L_p(f)$ are shallower than the $L_F(f)$ predicts and are thus underestimated, as seen in Figure 6b.

Similar trends are also identified in the $L_B(f)$ with increasing angle. The peak frequency and peak level of the $L_B(f)$ increase until approximately 60°, at which point the peak level begins to decrease. The width of the $L_B(f)$ remains relatively constant with increasing angle until 39°, at which point it narrows until it reaches 62°, where it begins to broaden once more. The trends identified in the behavior of the $L_B(f)$ agree with those found in Nielsen *et al.*[14], Tam *et al.*[15], and Vaughn *et al.*[10] However, beginning at approximately 73°, the width of the peak of the $L_p(f)$ becomes too wide for the $L_B(f)$ to capture by itself, and the peak appears to exhibit some behaviors more consistent with LSN. Thus, all three predictive models are used (see Figure 6c) to fit the measured spectra as accurately as possible. While no previous research has used both similarity spectra and a BSN model on the same spectrum, all three models are needed to identify the characteristics of both the mixing noise and the BSN present at this location.

The $L_F(f)$, $L_L(f)$, and $L_B(f)$ are used to match the shape of the $L_p(f)$ until approximately 89°, at which point only the $L_F(f)$ and $L_L(f)$ are needed. In Figure 6d, the $L_L(f)$ captures the sharper peak while the $L_F(f)$ captures the

shallower slopes. The $L_p(f)$ at low frequencies exhibit characteristics of microphone preamplifier saturation,[18,20] which can occur because of high-voltage, shock-like transients at higher-sensitivity microphones, and accounts for their atypical spectral behavior at those frequencies. At very high frequencies, however, a different source for the shallower slope is identified. Leete *et al.*[18] determined that, for afterburner conditions, the skewness of the pressure derivative (also known as derivative skewness) reached a value of 3 at approximately 3m downstream of the nozzle. As significant shock-like content present in the acoustic pressure waveforms (which appears in the form of shallower slopes at high frequencies) tends to occur at derivative skewness values above 3,[21,22] the shallower slope seen at the high frequencies in Figure 6d is due to the presence of shocks in the acoustic field. Schlinker *et al.*[23] also noticed a 5-7 dB/decade shallower slope at high frequencies that they attributed to the same phenomenon. These effects are evident in the measured spectra through the end of the array.

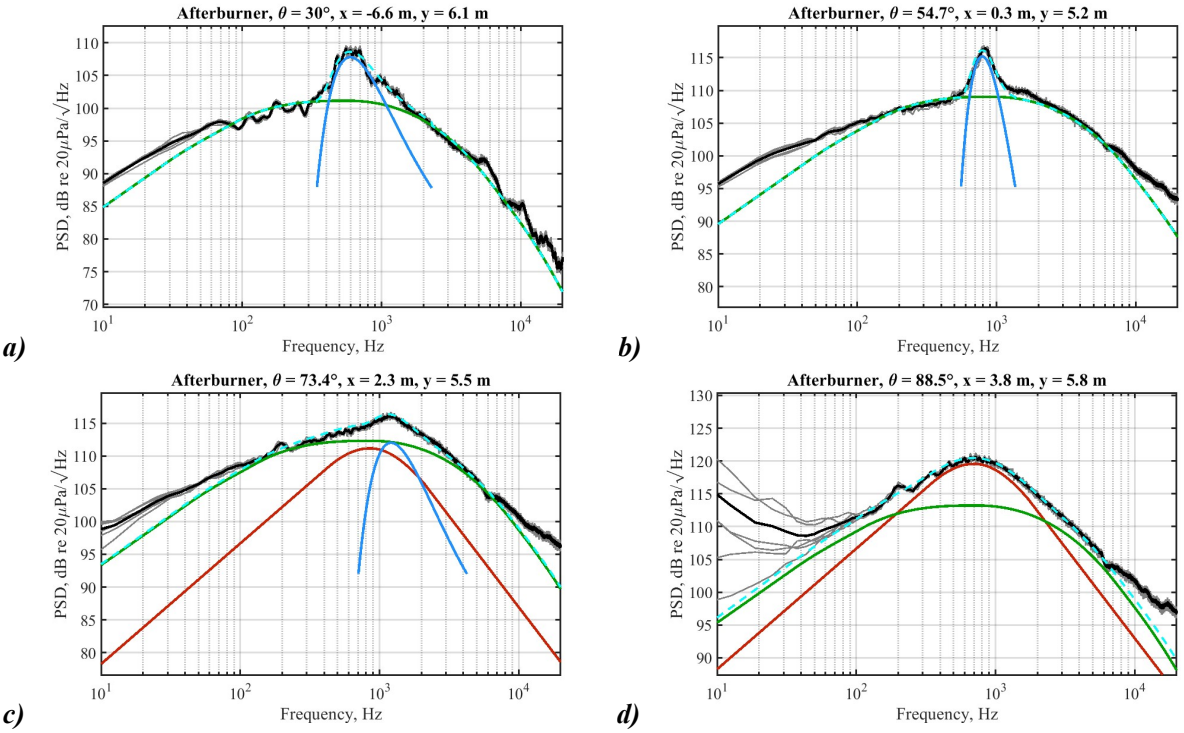

Figure 6. Measured and similarity spectra for 82% N2 consisting of gray lines ($L_p(f)$ of individual measurements), black lines ($L_p(f)$ of average of the 6 measurements), green lines ($L_F(f)$), red lines ($L_L(f)$), blue lines ($L_B(f)$), and cyan dashed lines (mix of $L_F(f)$, $L_L(f)$, and $L_B(f)$ or $L_F(f)$ and $L_L(f)$) at angles of a) 30°, b) 55°, c) 73°, d) 89°.

From angles 89° through 92°, only the $L_F(f)$ and $L_L(f)$ are applied to the measured spectra. Downstream of those angles, the shallower high-frequency slope of the measured spectra is most likely due to nonlinear propagation effects rather than FSN. The $L_L(f)$ is therefore the only model applied downstream of 92°, as shown in Figure 7a. There are also underestimations at low frequencies due to shallow slopes, but the cause of this effect is unknown. Trends in the peak frequency and peak level of the $L_L(f)$ are observed to be similar to those at the intermediate conditions. As inlet angle increases, the peak frequency decreases while the peak level increases until approximately 130°, at which point it begins to decrease.

Another phenomenon to note is the presence of multiple maxima and minima in the peak-frequency region of the measured spectra. These peaks are indicative of a "spatiospectral" lobing effect seen by Leete *et al.*[18] observed in previous full-scale studies[7,13,14,15] of high-performance aircraft, but their cause has yet to be definitively determined. Farther downstream, the multiple peaks detected evolve into two distinct peaks with a large null between them, as seen in Figure 7b. The high-frequency slope still exhibits the shallow slope due to the presence of shocks in the acoustic field, but the low-frequency slope steepens drastically until the predicted low-frequency slope of the $L_L(f)$ overestimates that of the $L_p(f)$. This steep slope is observed in the measured spectra until approximately 154°.

Near the end of the array, the effects of hydrodynamic factors are once again identified in the differing levels between runs. Figure 7c, which shows those effects, also shows an interesting spectral behavior not seen at the intermediate conditions. A null generates a second peak that shifts the high-frequency slope to frequencies higher than the $L_L(f)$ can predict, assuming the first peak in the $L_p(f)$ is a result of LSN. The two peaks shown in Figure 7c persist through the end of the array. This introduces an interesting dilemma in how to apply the $L_L(f)$ to the end of this array because of the uncertainty regarding where in the frequency domain the LSN has the greatest effect. In following the trend of the peak frequency decreasing in value with increasing inlet angle, as well as following the expected predictions of low-frequency noise dominating in the downstream region, the $L_L(f)$ is applied to the first peak in this analysis. Whether this is where the $L_L(f)$ should be applied or not is still uncertain. Tam and Parrish[7] identified similar behavior in their study of data from another installed engine, but a confirmed source of the second peak remains to be determined. At the end of the array (165°), the shapes of the $L_p(f)$ are still most likely affected by hydrodynamics and become less distinct, as is the case at the 82% N2 condition. There is a possible low-frequency peak to which the $L_L(f)$ has been fit, but the lack of a defined spectral shape makes this application less certain. A $L_L(f)$ spectral peak in the 200-300 Hz region could just as easily have been chosen.

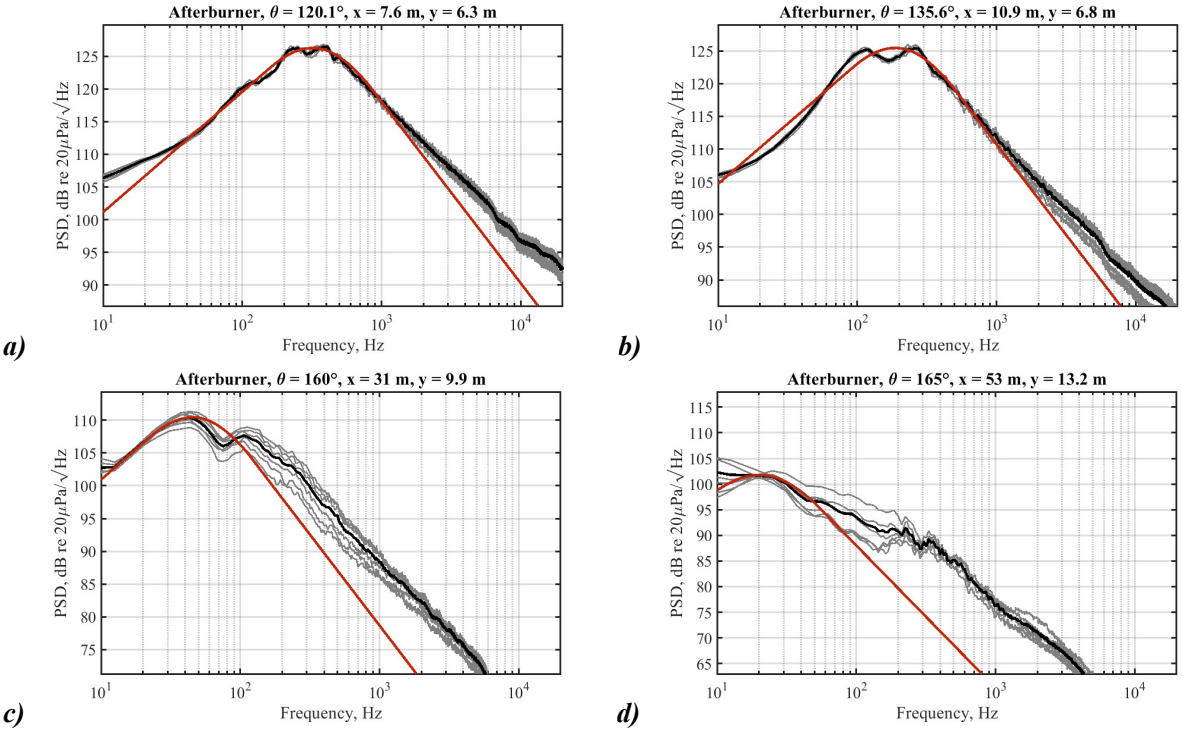

Figure 7. Measured and similarity spectra for 82% N2 consisting of gray lines (L_p(f) of individual measurements), black lines (L_p(f) of average of the 6 measurements), and red lines (L_L(f)) at angles of a) 120°, b) 136°, c) 160°, d) 165°.

4. DISCUSSION

Despite being developed from far-field, laboratory-scale data, Tam *et al.*'s similarity spectra[11] and Kuo *et al.*'s BSN model[6] appear to generally identify the behaviors of fine-scale noise (FSN), large-scale noise (LSN), and broadband shock-associated noise (BSN) in the measured spectra of a near-field ground array at 82% N2 and afterburner conditions. Performing this analysis helps confirm that the FSN dominates the upstream and sideline regions of the aircraft engine radiation, the LSN dominates downstream, and the BSN co-dominates with FSN at higher engine powers. A transition region consisting of FSN and LSN occurs just downstream of the nozzle for both engine conditions, with an additional transition region consisting of BSN and FSN and LSN occurring at afterburner. The peak frequency and peak level of the fine-scale similarity spectrum ($L_F(f)$) and the large-scale similarity spectrum ($L_L(f)$) show somewhat similar trends between the intermediate and afterburner

conditions across the entire array. For the $L_F(f)$, the peak frequency at 82% N2 decreases while at afterburner it increases and then decreases with increasing inlet angle. The peak level of the $L_F(f)$ increases then decreases with increasing angle for both conditions, but the point at which it decreases differs for each condition. For the $L_L(f)$, the peak frequency decreases and the peak level increases and then decreases for both engine powers. Once again, however, the angle at which the peak level of the $L_L(f)$ begins to decrease differs for each condition. The trends in the characteristics of the BSN spectral model ($L_B(f)$) match what was found by Neilsen *et al.*[14] at high engine powers. As inlet angle increases, the peak frequency increases and the peak level increases and then decreases. The width of the $L_B(f)$ remains relatively constant until 39°, at which point it decreases until it reaches an angle of 62° where it starts to increase.

Despite the overall There are three phenomena identified in this analysis that cannot be accounted for by the similarity spectra. The first of these is the disproportionate growth of the peaks compared to the high- and low-frequency slopes of the measured spectra at the 82% N2 condition. This type of behavior makes it impossible to fit the $L_L(f)$ to both the slopes and the peak region simultaneously. For angles 138° to 160°, the $L_L(f)$ is used to match the slopes of the measured spectra, underestimating the peak level by as much as 5-7 dB. This phenomenon has not been observed at intermediate engine powers in other studies, and the cause of this discrepancy remains unknown. Another phenomenon noted in this study is the presence of double peaks in the measured spectra at downstream locations for the afterburner engine condition. While no potential causes for this behavior have been identified or discussed in this paper, the analysis of this dataset contributes to the number of other studies[7,13,14,15] that have also seen double peaks in their spectra, thereby providing additional data for future studies on the subject. The third phenomenon noted in this study is the deterioration of the spectral shapes near the end of the array for both engine conditions. Because this study placed microphones farther downstream than other full-scale tests have done before, the lack of distinct, single-peaked spectra is a behavior not observed to date. Whether hydrodynamic factors, the lack of dominant LSN, or a different source of noise are the cause of this phenomenon is still unknown and requires further study.

This analysis of these three noise components provides a useful starting point in characterizing the sources of jet noise for this dataset on an installed GE F404-103 engine. Future work involving spatiospectral decompositions and comparisons to far-field data will provide further insight into the applicability of the similarity spectra analysis on full-scale field tests of high-performance aircraft and the phenomenological behavior observed in this paper.

ACKNOWLEDGMENTS

This analysis was funded under Office of Naval Research Grant No. N00014-21-1-2069 and by mentored research funds from Brigham Young University. Measurements were funded by the Air Force Research Laboratory. The Advanced Pilot Training Systems Program Office and Holloman Air Force Base are thanked for their cooperation in carrying out this study.

REFERENCES

[1] D. Casalino, F. Diozzi, R. Sannino, and A. Paonessa, "Aircraft Noise Reduction Technologies: A Bibliographic Review," Aerospace Science and Technology, Vol. 12, No. 1, 2008, pp. 1–17.

[2] Brenton Greska, Anjaneyulu Krothapalli, John M. Seiner, Bernard Jansen, and Laurence Ukeiley, "The Effects of Microjet Injection on an F404 Jet Engine," AIAA paper no. 2005-3047.

[3] John M. Seiner, Laurence S. Ukeiley, and Bernard J. Jansen, "Aero-performance Efficient Noise Reduction for the F404-400 Engine," AIAA paper no. 2005-3048.

[4] M. Samimy, K. B. M. Q. Zaman, and M. F. Reeder, "Effect of Tabs on the Flow and Noise Field of an Axisymmetric Jet," AIAA Journal, Vol. 31, No. 4, 1993, pp. 609–619.

[5] Christopher K. W. Tam, K. Viswanathan, K. K. Ahuja, and J. Panda, "The Sources of Jet Noise: Experimental Evidence," J. Fluid Mech., Vol. 615, 2008, pp. 253-292.

[6] Ching-Wen Kuo, Dennis K. McLaughlin, Philip J. Morris, and K. Viswanathan, "Effects of Jet Temperature on Broadband Shock-Associated Noise," AIAA Journal, Vol. 53, No. 6, 2015, pp. 1515-1530.

[7] Christopher K. W. Tam and Sarah A. Parrish, "Noise of High-Performance Aircraft at Afterburner," Journal of Sound and Vibration, Vol. 352, 2015, pp. 103-128.

[8] M. K. Ponton and J. M. Seiner, "The Effects of Nozzle Exit Lip Thickness on Plume Resonance," Journal of Sound and Vibration, Vol. 154, No. 3, 1992, pp. 531-549.

[9] J. Panda, "An Experimental Investigation of Screech Noise Generation," J. Fluid Mech., Vol. 378, 1999, pp. 71-96.

[10] Aaron B. Vaughn, Tracianne B. Neilsen, Kent L. Gee, Alan T. Wall, J. Micah Downing, and Michael M. James, "Broadband Shock-Associated Noise from a High-Performance Military Aircraft," JASA, Vol. 144, No. 3, 2018, pp. EL242–EL247.

[11] Christopher K. W. Tam, Michel Golebiowski, and J. M. Seiner, "On the Two Components of Turbulent Mixing Noise from Supersonic Jets," AIAA paper no. 1996-1716.

[12] Blaine M. Harker, Kent L. Gee, Tracianne B. Neilsen, Alan T. Wall, Sally A. McInerny, and Michael M. James, "On Autocorrelation Analysis of Jet Noise," JASA, Vol. 133, No. 6, 2013, pp. EL458-EL464.

[13] Tracianne B. Neilsen, Kent L. Gee, Alan T. Wall, and Michael M. James, "Similarity Spectra Analysis of High-Performance Jet Aircraft Noise," JASA, Vol. 133, No. 4, 2013, pp. 2116-2125.

[14] Tracianne B. Neilsen, Aaron B. Vaughn, Kent L. Gee, S. Hales Swift, Alan T. Wall, J. Micah Downing, and Michael M. James, "Three-Way Spectral Decompositions of High-Performance Military Aircraft Noise," AIAA Journal, Vol. 57, No. 8, 2019, pp. 3467-3479.

[15] Christopher K. W. Tam, Allan C. Aubert, John T. Spyropoulos, and Russell W. Powers, "On the Dominant Noise Components of Tactical Aircraft: Laboratory to Full Scale," AIAA paper no. 2017-3516.

[16] Tracianne B. Neilsen, Kent L. Gee, Blaine M. Harker, and Michael M. James, "Level-educed Wavepacket Representation of Noise Radiation from a High-performance Military Aircraft," AIAA paper no. 2016-1880.

[17] GE Aviation, "F404 Turbofan Engines," https://www.geaviation.com/sites/default/files/datasheet-F404-Family.pdf

[18] Kevin M. Leete, Aaron B. Vaughn, Michael S. Bassett, Reese D. Rasband, Daniel J. Novakovich, Kent L. Gee, S. Conner Campbell, Frank S. Mobley, and Alan T. Wall, "Jet Noise Measurements of an Installed GE F404 Engine," AIAA paper no. 2021-1638.

[19] Aaron B. Vaughn, Tracianne B. Neilsen, Kent L. Gee, Koji Okamoto, and Masahito Akamine, "Near-Field Spatial Variation in Similarity Spectra Decomposition of a Mach 1.8 Laboratory-Scale Jet," Proc. Mtgs. Acoust. **29**, 045004 (2016).

[20] Troy Taylor, Kent L. Gee, Jarom H. Giraud, Scott D. Sommerfeldt, Jonathan D. Blotter, and Curtis P. Wiederhold, "On the Use of Prepolarized Microphone Systems in Rocket Noise Measurements," Proc. Mtgs. Acoust. **14**, 040005 (2012).

[21] Brent O. Reichman, Michael B. Muhlestein, Kent L. Gee, Tracianne B. Neilsen, and Derek C. Thomas, "Evolution of the Derivative Skewness for Nonlinearly Propagating Waves," JASA, Vol. 139, No. 3, 2016, pp. 1390-1403.

[22] Kent L. Gee, Paul B. Russavage, Tracianne B. Neilsen, S. Hales Swift, and Aaron B. Vaughn, "Subjective Rating of the Jet Noise Crackle Percept," JASA, Vol. 144, No. 1, 2018, pp. EL40-EL45.

[23] R. H. Schlinker, S. A. Liljenberg, D. R. Polak, K. A. Post, C. T. Chipman, and A. M. Stern, "Supersonic Jet Noise Characteristics and Propagation: Engine and Model Scale," AIAA paper no. 2007-3623.